Materials Science & Engineering C 107 (2020) 110266

Contents lists available at ScienceDirect

Materials Science & Engineering C

journal homepage: www.elsevier.com/locate/msec

How biomimetic amino modified mesoporous silica xerogel regulates loading and in vitro sustained delivery of levorotary ofloxacin

Ping Zhang, Tong Lu, Xiaojie Xia, Lingqiong Wu, Long Shao, Jiahua Zhou, Jing Li*

School of Basic Medical Science, Shenyang Medical College, Shenyang, China

ARTICLE INFO

Keywords:
Amino modified mesoporous silica
Levorotary ofloxacin
Box–behnken experimental design

ABSTRACT

The purpose of this study was to facilely develop biomimetic amino modified mesoporous silica xerogel (AMSX) and study how AMSX regulated loading and in vitro sustained delivery of carboxyl-containing drug levorotary ofloxacin (LOFL). Characteristics of AMSX, including morphology, porous structure, elements and crystalline state were investigated and pharmaceutical performance of AMSX for the delivery of LOFL was studied. The result showed that AMSX was accumulational spherical nanoparticles with mesoporous structure. Hydrogen bonding force was formed between carboxylic groups of LOFL and amino groups grafted on the surface of AMSX. Furthermore, a three-level three-factorial Box–Behnken experimental design was applied to optimize the amount of major agent for synthesizing AMSX with expected drug loading capacity and also to figure out how AMSX regulated in vitro delivery of LOFL. It is believed that the present work will provide novel insights for designing mesoporous silica as drug carrier and favored the development of sustained release system.

1. Introduction

It is widely known that porous materials inorganic nanomaterials have important adsorption applications [1–3]. Among them, nanoporous silica with amorphous state has been long recognized as promising excipient for drug delivery application owing to its simple, inexpensive, versatile synthesis, physiologically inert and non-toxic characteristics. There are three types of nanoporous silica structures: micropores (pore diameters of less than 2 nm), mesopores (pore diameters between 2 and 50 nm), and macropores (pore diameters greater than 50 nm) based on the diameter of the pores [4–6]. Up to now, mesoporous silica materials with different pore characteristics and a variety of morphologies have been widely described, where different kinds of drug molecules have been successfully incorporated [7–10]. Among so many methods of synthesizing mesoporous silica, biomimetic synthesis has attracted great attention in recent years [11,12]. There are a number of amine-containing molecules, including polypeptides, synthesized polymers/oligomers and small molecules, have been explored for the biomimetic synthesis of silica [13]. Recently, biomimetic synthesis of mesoporous silica mediated by polyamines has attracted great attention [14,15]. Polyamines catalyze the silica formation due to the alternating presence of protonated and nonprotonated amine groups in the polyamine chains to form hydrogen bonds with the oxygen adjacent to silicon [16].

Levorotary ofloxacin (LOFL, see Fig. 1), a water-soluble fluoroquinolone antibiotic, is widely used in human veterinary medicines and aquatic breeding [17]. Sustained release formulation of LOFL can exert function for a long time and reduce frequency of drug administration. In the present work, amino modified mesoporous silica xerogel (AMSX) was facilely synthesized using co-condensation method with branched poly(ethyleneimine)s (PEIs) as the template and 3-Aminopropyltriethoxysilane (APTES) as amino functional species. The purpose of amino modification of mesoporous silica xerogel was to (1) accelerate polycondensation process because amine groups catalyze condensation of silica precursors [18]; (2) improve loading capacity of drug molecules with carboxyl-containing group due to the strong hydrogen bonding force formed between amino groups with carboxylic group of drug molecules [19]. Thus, AMSX was designed as carrier for LOFL (LOFL has carboxylic group) and the pharmaceutical performance of AMSX for the delivery of LOFL was studied.

Though there are a large number of literatures report the application of mesoporous silica as drug carrier [20–24], the application of proper experimental design to study how influencing factors affect application performance has rarely been reported. For the first time, a three-level three-factorial Box–Behnken experimental design was applied to optimize the amount of major agent for synthesizing AMSX with expected application (including reduction of burst release, sustaining LOFL for 24 h and high LOFL loading capacity). Box-Behnken

* Corresponding author. No. 146 Huanghe North Street, Shenyang, Liaoning Province, China.
E-mail address: dddefghijklmn@163.com (J. Li).

https://doi.org/10.1016/j.msec.2019.110266
Received 18 December 2018; Received in revised form 7 September 2019; Accepted 29 September 2019
Available online 01 November 2019

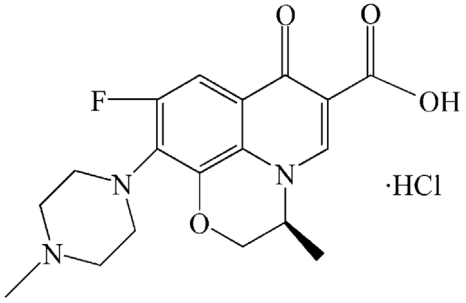

Fig. 1. Chemical structure of model drug LOFL.

statistical design is an independent, rotatable or nearly rotatable, quadratic design, which requires less experimental runs and time. Therefore, it can be considered as a cost-effective technique than other usual processes to analyze how parameters influence independent variables then to optimize expected synthesized carrier materials for formulation [25,26]. In the present work, optimized AMSX samples were made, and then drug loading capacity and in vitro release experiment were conducted to verify the predictability of the applied Box–Behnken experimental design. The advantage of optimized delivery system of LOFL-AMSX was to sustain LOFL release for 24 h and achieve relative low burst release as well as high drug loading capacity. However at present, it should admit that there are some practical issues in accomplishing the in vivo study of drug loaded AMSX systems, especially the systemic safety pre-evaluation of in vivo tests on beagle dogs.

2. Materials and methods

2.1. Materials

Tetramethoxysilane (TMOS) and 3-aminopropyltriethoxysilane (APTES) were purchased from Aladdin (Shanghai, China), branched poly(ethyleneimine)s (PEIs) with weight-average molecular weight of 20 kDa was kindly donated by Qianglong new chemical materials (Wuhan, China). Deionized water was prepared by ion exchange.

2.2. Facile preparation of AMSX

AMSX was facilely synthesized with co-condensation method using PEIs as the template. Before preparation, PEIs was dissolved in aqueous solution and the template solution was left statically for more than 24 h. Afterwards, 0.5 ml as-synthesized template solution was added into mixed solution consisting of 0.5 ml TMOS, 0.5 ml absolute ethyl alcohol and 50 μl APTES, and left the colloidal system at ambient conditions statically until the formation of wet gel. Finally, wet gel was dried at 40 °C vacuum drying oven to remove volatile solvent.

2.3. Characterization of AMSX

The surface morphology of AMSX was characterized using SURA 35 field emission scanning electron microscope (ZEISS, Germany). Samples were mounted onto metal stubs by double-sided adhesive tape and sputtered with a thin layer of gold under vacuum. The porous structure of AMSX was characterized using a Tecnai G2 F30 TEM instrument (FEI, The Netherlands) operated at 200 kV. Before examination, samples were dispersed in deionized water through sonication and subsequently deposited on carbon-coated copper grids. The crystalline state of AMSX was evaluated with differential scanning calorimeter (DSC, Q1000, TA Instrument, USA). Samples were placed in pierced aluminum pans and heated from 30 to 300 °C at a scanning rate of 10 °C/min under nitrogen protection. The surface area and pore volume of AMSX were studied by determining the nitrogen adsorption/desorption using a SA3100 surface area and pore size analyzer (Beckman Coulter, USA). The specific surface area (S_{BET}) was evaluated from nitrogen adsorption data over the relative pressure range from 0.05 to 0.2 using the Brunauer–Emmett–Teller (BET) method. Pore size distributions (PSDs) were determined from adsorption branches of isotherms with the Barrett–Joyner–Halenda (BJH) method. The total pore volume (V_t) was determined from the amount adsorbed at a relative pressure of 0.99. XPS spectrum of AMSX was analyzed using Thermo K-alpha spectrometer with hemispherical analyzer. The XPS analysis of several comparable samples (sample 1, sample 2, sample 3, sample 4, sample 11 and sample 12) with different amount of APTES as amino functional agent and various sample sizes was also conducted and the result was displayed in supporting information Table 3. Amino group amount on the silica matrix of these comparable samples was determined using acid-base titration method according to Ref. [5]. Briefly, 0.1 g carrier was added to 4.0 ml 0.01 M HCl standard solution (0.01 M). The system was stirred, centrifuged, washed with distilled water and finally collected the supernatant. Afterwards, phenolphthalein solution was mixed with supernatant solution, and NaOH solution (0.01 M) was applied to titrate. The volume of NaOH used was recorded when the color changed from colorless to pink and this conversion can keep for 30 s. Amino group content was calculated according to the following equation.

$$\text{Amino group content(mmol/g)} = \frac{0.01*(4.0 - V)}{0.1}$$

2.4. Drug loading procedure

Drug loading procedure was carried out with in situ drug inclusion method. Briefly for drug loading procedure, 100 mg LOFL was dissolved in 0.5 ml deionized water, which was named as LOFL aqueous solution. Afterwards, the LOFL aqueous solution was added into the gelling solution that consisted of 0.5 ml TMOS, 0.5 ml absolute ethyl alcohol, 0.5 ml PEIs aqueous solution (0.4 ml PEIs was dissolved in 40.8 ml deionized water) and 50 μl APTES. Finally, the system was vortex for 3min, left statically until the formation of wet gel and dried at 40 °C vacuum drying oven to get LOFL-AMSX. Drug loading capacity was measured by taking an accurately weighed quantity of LOFL-AMSX, then extracting the loaded LOFL completely using deionized water under ultrasound, and finally measuring drug content with ultraviolet spectroscopy (UV-1750, Shimadzu, Japan) at the wavelength of 292 nm. The drug loading capacity can be calculated using the following equation [27]:

$$\text{Drug loading(\%)} = \frac{\text{Weight of drug in carrier}}{\text{Weight of carrier}} \times 100$$

2.5. FTIR

To examine the interaction forces formed between drug (LOFL) and carrier (AMSX), FTIR (Spectrum 1000, PerkinElmer, USA) spectra of samples were obtained over the spectral region 400–4000 cm^{-1}. Samples were prepared by respectively grounding AMSX, LOFL and LOFL-AMSX with KBr.

2.6. In vitro drug dissolution of LOFL-AMSX

In vitro dissolution experiment was carried out using USP paddle method (100 rpm, 37 °C) with a ZRD6-B dissolution tester (Shanghai Huanghai Medicament Test Instrument Factory, China). Samples were exposed to simulated gastric fluid (SGF, pH 1.0 hydrochloric acid). At predetermined time intervals, 5 ml dissolution medium was withdrawn from the release medium and then an equivalent amount of fresh medium was added to maintain a constant dissolution volume. The withdrawn dissolution medium was administered through 0.45 μm

Table 1
Variables in Box–Behnken experimental design.

Factor	Level		
	−1	0	+1
X_1 APTES (μl)	20	50	100
X_2 PEI (ml)	0.2	0.5	1.0
X_3 TMOS (ml)	0.2	0.5	1.0
Response	Constraints		
Y_1 Cumulative release in 1 h	Minimize		
Y_2 Cumulative release in 24 h	Maximize		
Y_3 Drug loading capacity (%)	Maximize		

microporous membrane then analyzed using UV-1750 (Shimadzu, Japan) at the wavelength of 294 nm.

2.7. Regulation of AMSX for loading and in vitro release of LOFL

A three-level three-factorial Box–Behnken experimental design (Design Expert, Version 8.0.6, Stat-Ease Inc., Minneapolis, MN) was used to evaluate the effects of major agent used (the amount of APTES, PEI and TMOS) as variables on the responses to optimize AMSX with desired functions as drug carrier. The design consists of center points and the set of points lying at themed point of each edge that defines the region of interest. The factors chosen and settings of factor levels were presented in Table 1.In the present study, 17 experiments were conducted in one block (Table 2). The selected responses were cumulative drug release in 1 h (Y_1), cumulative drug release in 24 h (Y_2) and drug loading capacity (Y_3). Low cumulative drug release in 1 h aimed to reduce burst release and high cumulative drug release at 24 h was favorable for clinical application of sustained release formulation. After optimization, optimized AMSX samples were made, and then drug loading capacity and in vitro release experiment were conducted.

2.8. Wettability measurement

Since drug loaded AMSX can be considered to be solid dispersions with AMSX as unsoluble excipient, wettability measurement was conducted to study its interfacial wetting behavior. The contact angle of optimized LOFL-AMSX was measured using the operation manual for automatic contact angle meter model JCY series (Shanghai, China).

Table 2
Observed responses for the Box–Behnken design. X_1 is factor of APTES amount (μl), X_2 is factor of PEI amount (ml), X_3 is factor of TMOS amount (ml), Y_1 is response of cumulative drug release in 1 h (%), Y_2 is response of cumulative drug release in 24 h (%), Y_3 is response of drug loading capacity (%).

Run	X_1	X_2	X_3	Y_1	Y_2	Y_3
1	20	0.2	0.5	70.4	100.0	16.0
12	50	1.0	1.0	53.3	100.0	11.6
3	20	1.0	0.5	57.5	100.0	10.8
6	100	0.5	0.2	58.7	100.0	28.5
15	50	0.5	0.5	80.7	100.0	12.3
17	50	0.5	0.5	80.7	100.0	12.4
2	100	0.2	0.5	78.3	100.0	19.7
13	50	0.5	0.5	80.7	100.0	12.2
4	100	1.0	0.5	55.7	100.0	18.6
11	50	0.2	1.0	76.4	86.9	12.7
9	50	0.2	0.2	60.6	100.0	15.6
16	50	0.5	0.5	80.8	100.0	12.2
7	20	0.5	1.0	53.0	85.2	10.2
14	50	0.5	0.5	82.1	100.0	12.0
8	100	0.5	1.0	62.9	90.5	12.4
10	50	1.0	0.2	71.3	100.0	14.9
5	20	0.5	0.2	66.0	100.0	13.5

200 mg AMSX powder that had been sieved was weighed and compressed using a steel punch and die assembly in a infrared tablet press under pressure. A drop of deionized water (20 μl) was put on the compressed plate and contact angle was measured every 1 s until the contact angle turned to zero.

3. Results and discussions

3.1. Characteristics of AMSX

The morphology and porous structure of AMSX were analyzed using scanning electron microscope (SEM) and transmission electron microscope (TEM). SEM micrograph (Fig. 2A) showed that AMSX was quite small nanoparticles aggregated intensively due to xerogel state. The TEM image of AMSX(Fig. 2B) confirmed the existence of disordered mesopores. Overall, DSC thermogram of AMSX (Fig. 2C) displayed no peak, indicating that AMSX was amorphous state and was safe to be used as drug carrier because crystalline silica is known to cause a rapid influx of inflammatory cells, increase collagen deposition in lungs, and change histological state of pulmonary lymph nodes, but not for amorphous silica [4]. It was worth noticing that endothermic phenomenon was shown due to the decomposition of aminopropyl groups during heat treatment. The reason was that the organic group of aminopropyl decomposed during measurement while not for inorganic silica [28]. Nitrogen adsorption/desorption isotherm and pore size distribution curve of AMSX were presented in Fig. 2D. The nitrogen adsorption/desorption isotherm of AMSX was type IV isotherm with a hysteresis loop according to the IUPAC classification [29–32]. The pore diameter of AMSX was 3.2 nm, which also confirmed the mesopores of AMSX. According to Fig. 2E and supporting information Table 2, XPS analysis evidenced the presence of carbon, oxygen, nitrogen and silicon elements in AMSX. Generally, carbon, oxygen, nitrogen and silicon elements content were within the range of 40–42 at%, 32–34 at%, 4–5 at% and 20–22 at%, respectively. XPS confirmed that AMSX contained nitrogen element, which gave hint that amino groups can be introduced in AMSX.

3.2. FTIR

FTIR spectra of AMSX, LOFL and LOFL-AMSX were shown in Fig. 3. FTIR spectrum of AMSX displayed a band assigned to NH_2 bending vibration at 1464.2 cm^{-1} and two bands assigned to CH_2 stretching due to the methyl groups introduced from aminopropyl groups of APTES at 2919.1 and 2850.4 cm^{-1} [33], which further confirmed the amino modification of AMSX. LOFL spectra exhibited its characteristic peak of acid carbonyl groups at 1623.5 cm^{-1}. After loading LOFL into AMSX, the spectrum showed disappearance of acid carbonyl stretching peak and the reduction of NH_2 bending vibration peak, possibly suggesting that the acid functional group of LOFL was involved in hydrogen bonding with the amino groups modified on the silica surface of AMSX [5,34,35] and further demonstrating the significance of amino modification for mesoporous silica xerogel as drug carrier.

3.3. LOFL loading and release principles

According to the parameters of several comparable carriers in supporting information Table 1, it was obvious that LOFL loading efficiency correlated with both amino group amount and sample size. The sample size result was shown in Table 5. AMSX size was determined by measuring their height and three kinds of size were defined according to the height range: small size (1.5–2.0 cm), medium size (2.1–2.5 cm) and large size (2.6–3.0 cm). The result demonstrated that when the sample sizes were similar, the more amino groups on the silica matrix, the higher LOFL loading capacity. If sample sizes significantly varied, the higher sample size, the lower drug loading capacity. In this case, amino group almost had no effect on LOFL loading capacity. As for

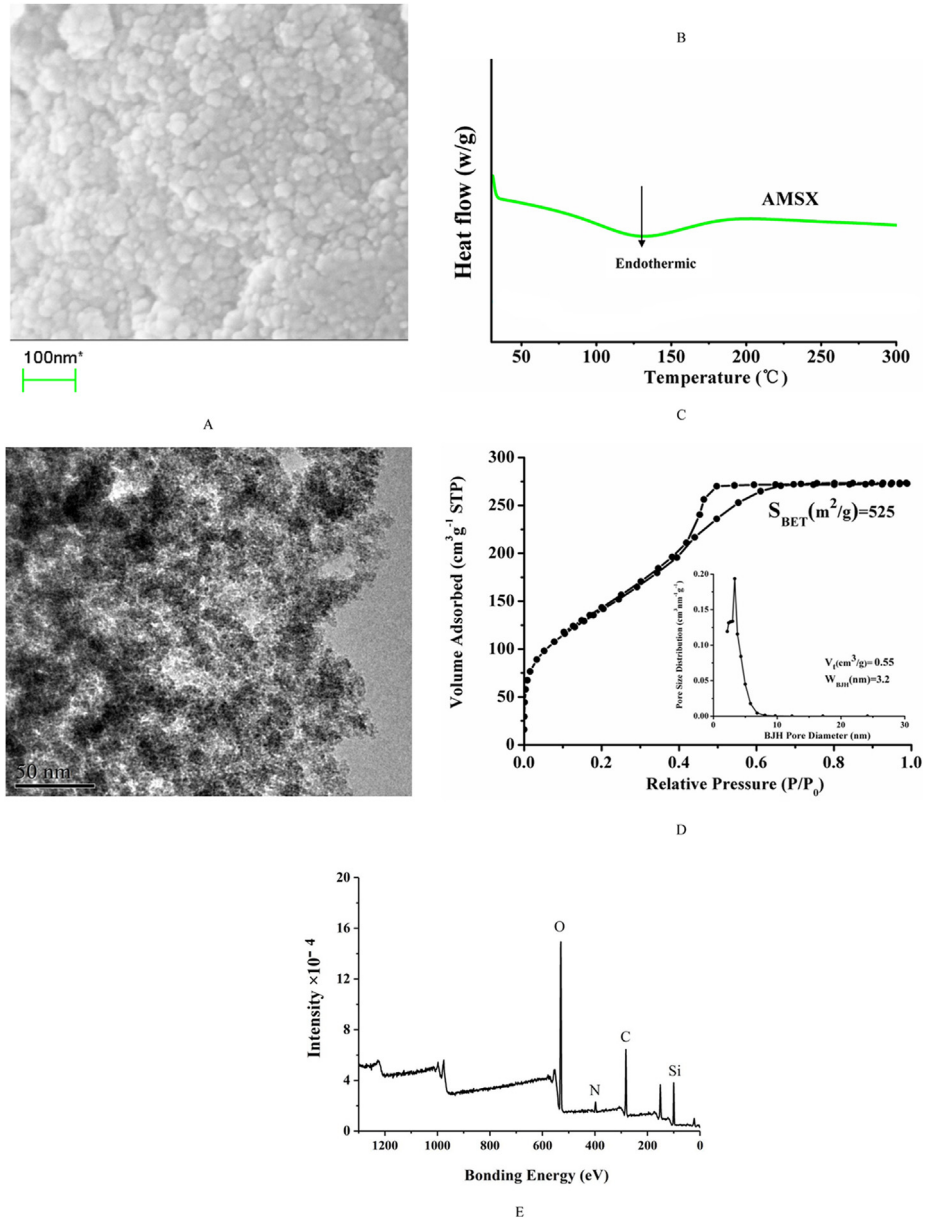

Fig. 2. A, SEM photograph of AMSX; B, TEM photograph of AMSX; C, DSC thermogram of AMSX; D, Nitrogen adsorption/desorption isotherm and pore size distribution curve of AMSX; E, XPS spectrum of AMSX.

LOFL release, the main influencing factor ascribed to pore size of carrier, and amino modification almost had no impact on drug release. LOFL released faster as increasing the pore size of carrier. In addition, the relationship between drug loading and carrier structure (surface area, pore volume and pore size) was also studied (see supporting information Table 2). Generally, surface area, pore volume and pore size were obviously lowered after loading LOFL, demonstrating that LOFL was sufficiently encapsulated into the pores of carrier, which agreed with most published works [19,27,34]. Furthermore, drug loading capacity almost positively correlated with reduced surface area. It was clear that the higher drug loading capacity, the larger surface area reduction, demonstrating that the efficient drug loading occupied large surface area of carrier.

3.4. Box–Behnken experimental design

3.4.1. Model fitting

Photo image of 17 AMSX samples was displayed in Fig. 4 and showed that AMSX samples had good moldability. The difference in their xerogel size can be observed. According to the fit summary for each response shown in Table 3, the cumulative drug release in 1 h was fitted to quadratic model, cumulative drug release in 24 h was fitted to both linear model and quadratic model, and drug loading capacity was fitted to linear model. For estimation of significance of these models, the analysis of variance (ANOVA) was applied (Table 4). It turned out that the experimental responses of model fitting were significant. The resulted equations and the corresponding R^2–values were presented below:

$$Y_1 = +19.06 + 0.8808X_1 + 47.77X_2 + 90.66X_3 - 0.1853X_1X_2 + 0.2159X_1X_3 - 44.16X_2X_3 - 7.253e^{-3}X_1^2 - 23.55X_2^2 - 68.08X_3^2,\ R^2 = 0.9188 \quad (1)$$

$$Y_2 = +102.4 + 0.1055X_1 - 15.90X_2 - 0.7068X_3 - 0.02446X_1X_2 + 0.07339X_1X_3 + 23.88X_2X_3 - 9.642e^{-4}X_1^2 + 6.849X_2^2 - 23.46X_3^2,\ R^2 = 0.9432 \quad (2)$$

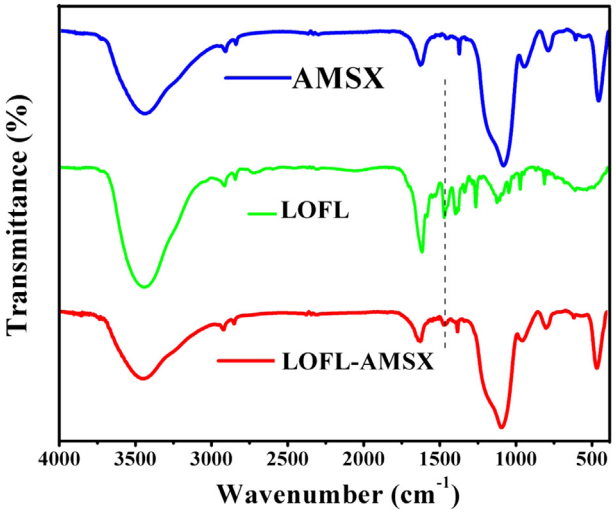

Fig. 3. FTIR spectra of AMSX, LOFL and LOFL-AMSX.

$$Y_3 = +14.35 + 0.09767X_1 - 2.127X_2 - 7.468X_3,\ R^2 = 0.6447 \quad (3)$$

A significant interaction effect of X_2X_3 was observed for responses of Y_1 and Y_2, which was favorable for both Y_1 (low value of Y_1 to reduce burst release) and Y_2 (high value of Y_2 to accomplish release in 24 h). In order to explain this specifically, some data in Table 2 has been reorganized to produce Table 5. AMSX size was determined by measuring their height and three kinds of size were defined according to the height range: small size (1.5–2.0 cm), medium size (2.1–2.5 cm) and large size (2.6–3.0 cm). It was obvious that when using the same amount of APTES, AMSX synthesized with higher X_2X_3 possessed larger xerogel size and lower drug loading capacity. For example, X_2X_3 of sample 3 was higher than sample 5 led to larger xerogel size of sample 3 than sample 5 and further resulted in lower drug loading capacity of sample 3 than sample 5. In this case, the initial LOFL release in 1 h can be reduced because the larger xerogel with the entrapment of smaller amount of drug molecules sustained drug release. It was also worth noticing that X_1 was positively linear correlation with Y_3, demonstrating that APTES showed positive impact on LOFL loading capacity because the higher amount of amino groups grafted onto the mesoporous silica had the ability to load larger amount of carboxyl-containing drug molecules through strong hydrogen bonding [19].

3.4.2. Contour plots and response surface analysis

For response surface design, the perturbation plots(Fig. 5) demonstrated how the response changed as each factor moved from the chosen level, with all other factors held constant at level zero. Overall, the three factors produced different effects on responses. It was shown that factor X_2 had negative effect on response Y_1 and Y_3, indicating that a small amount of PEI was sufficient to synthesize AMSX since the polymer PEI had strong reaction ability to interact with silicon hydroxyl groups. Two-dimensional contour plots and three dimensional response surface plots, as presented in Fig. 6 and Fig. 7, were very useful to comprehend the interaction of factors on the responses. In all the presented figures, the third factor was kept at level zero. In the case of response Y_3, the almost straight lines in Fig. 6 predicted nearly linear relationship between factor X_1, factor X_2 and factor X_3. However, all the relationships among the three variables in the case of Y_1 and Y_2 were non-linear, which were shown even more clearly in response surface plots. This phenomenon revealed that the three factors had strong interaction effect with each other. According to two-dimensional contour plots and three dimensional response surface plots of responses Y_2 AC and Y_2 BC, low dosage of TMOS was favorable to obtain maximize

Table 3
Fit summary for responses Y_1, Y_2 and Y_3. Y_1 is response of cumulative drug release in 1 h (%), Y_2 is response of cumulative drug release in 24 h (%), Y_3 is response of drug loading capacity (%).

Source	Y_1		Y_2		Y_3	
	F Value	P-value Prob > F	F Value	P-value Prob > F	F Value	P-value Prob > F
Sequential Model Sum of Squares						
Linear	1.24	0.3336	6.79	0.0054	7.86	0.0030
2FI	0.78	0.5326	2.67	0.1047	2.35	0.1335
Quadratic	15.76	0.0017	6.55	0.0193	3.33	0.0862

Table 4
The analysis of variance for responses Y_1, Y_2 and Y_3. X_1 is factor of APTES amount (μl), X_2 is factor of PEI amount (ml), X_3 is factor of TMOS amount (ml), Y_1 is response of cumulative drug release in 1 h (%), Y_2 is response of cumulative drug release in 24 h (%), Y_3 is response of drug loading capacity (%).

Source	Y_1		Y_2		Y_3	
	F Value	P-value Prob > F	F Value	P-value Prob > F	F Value	P-value Prob > F
Model	8.80	0.0045	12.91	0.0014	7.86	0.0030
X_1	0.45	0.5236	1.35	0.2840	14.48	0.0022
X_2	17.90	0.0039	9.94	0.0161	0.69	0.4221
X_3	1.14	0.3213	38.23	0.0005	8.47	0.0122
X_1X_2	1.69	0.2350	0.20	0.6654	–	–
X_1X_3	2.29	0.1738	1.81	0.2208	–	–
X_2X_3	9.59	0.0174	19.13	0.0033	–	–
X_1^2	21.82	0.0023	2.63	0.1488	–	–
X_2^2	2.30	0.1731	1.33	0.2870	–	–
X_3^2	19.22	0.0032	15.58	0.0056	–	–

Table 5
Reorganized data mainly according to Table 2. X_2 is factor of PEI amount (ml), X_3 is factor of TMOS amount (ml).

APTES (μl)	Run	Drug loading capacity (%)	X_2X_3	AMSX size
20	1	16.0	0.1	Small
	5	13.5	0.1	Small
	3	10.8	0.5	Large
	7	10.2	0.5	Large
50	9	15.6	0.04	Small
	10	14.9	0.2	Medium
	11	12.7	0.2	Medium
	13	12.2	0.25	Medium
	12	11.6	1.0	Large
100	2	19.7	0.1	Small
	6	28.5	0.1	Medium
	4	18.6	0.5	Large
	8	12.4	0.5	Large

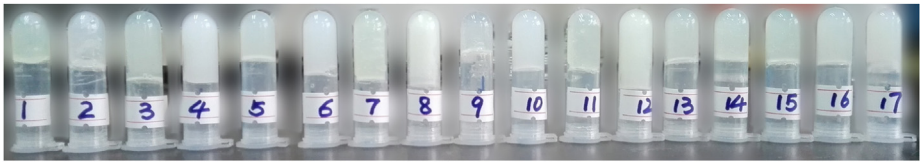

Fig. 4. Photo image of 17 AMSX samples for Box–Behnken experimental design.

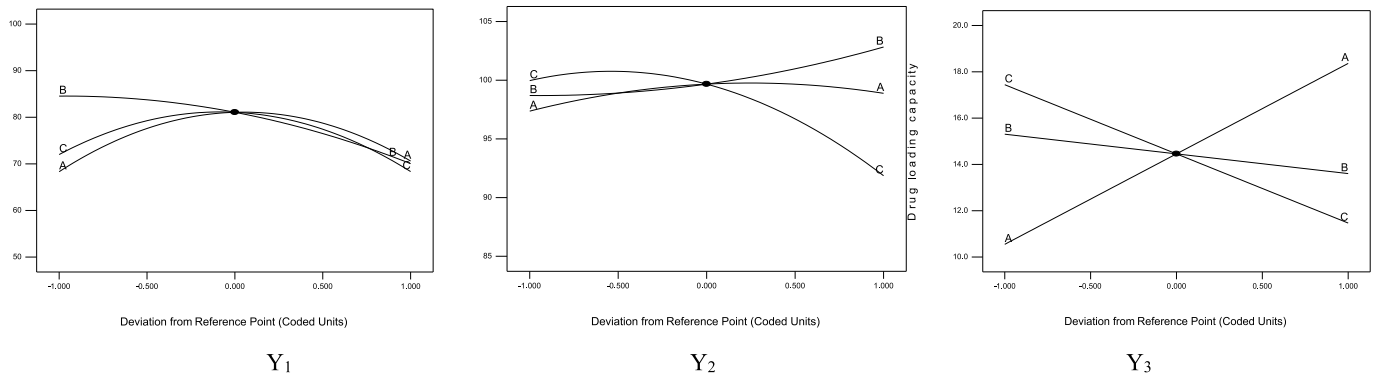

Fig. 5. Perturbation plots showing effects of X_1 (A), X_2 (B) and X_3 (C) on responses Y_1, Y_2 and Y_3. X_1 is factor of APTES amount (μl), X_2 is factor of PEI amount (ml), X_3 is factor of TMOS amount (ml), Y_1 is response of cumulative drug release in 1 h (%), Y_2 is response of cumulative drug release in 24 h (%), Y_3 is response of drug loading capacity (%).

cumulative release in 24 h. The reason was that when the same amount of APTES and PEI were used in synthesized process, drug loading capacity increased with the reduction of TMOS, thus increasing cumulative release in 24 h. This also reflected that TMOS could efficiently incorporate drug molecules with low dosage due to its strong hydrolysis and polycondensation properties. On the contrary, higher dosage of TMOS loaded less drug molecules because the same amount of drug molecules can be encapsulated more sparsely in resulted larger xerogel carrier.

3.4.3. Optimization

The optimized AMSX was selected based on the criteria of attaining the minimum cumulative drug release in 1 h (Y_1) to reduce burst release and the maximum cumulative drug release in 24 h (Y_2) to prolong sustained release, while maximizing the drug loading capacity (Y_3) to highlight the advantages of AMSX as carrier. The optimized compositions were presented in Table 6. In practical, optimized sample 1 and 2 were failed to prepare and only sol state can be obtained, which attributed to the insufficient of silica framework with low dosage of TMOS. When the consumption of TMOS reached to 50 μl, the synthesized sample formed gel state and then xerogel state after being dried.

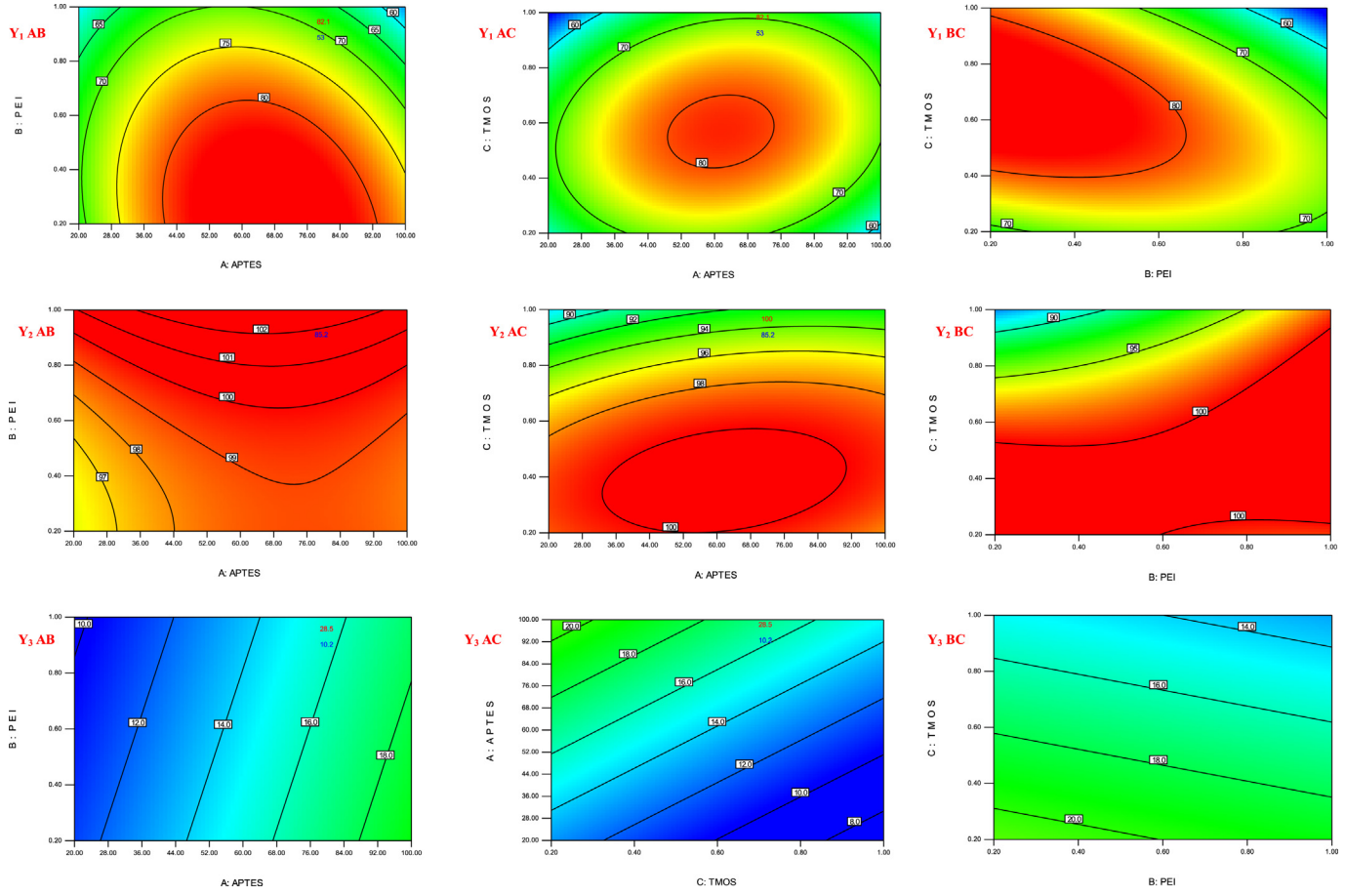

Fig. 6. Contour plots showing effects of various independent variables on response Y_1, Y_2 and Y_3. X_1 is factor of APTES amount (μl), X_2 is factor of PEI amount (ml), X_3 is factor of TMOS amount (ml), Y_1 is response of cumulative drug release in 1 h (%), Y_2 is response of cumulative drug release in 24 h (%), Y_3 is response of drug loading capacity (%).

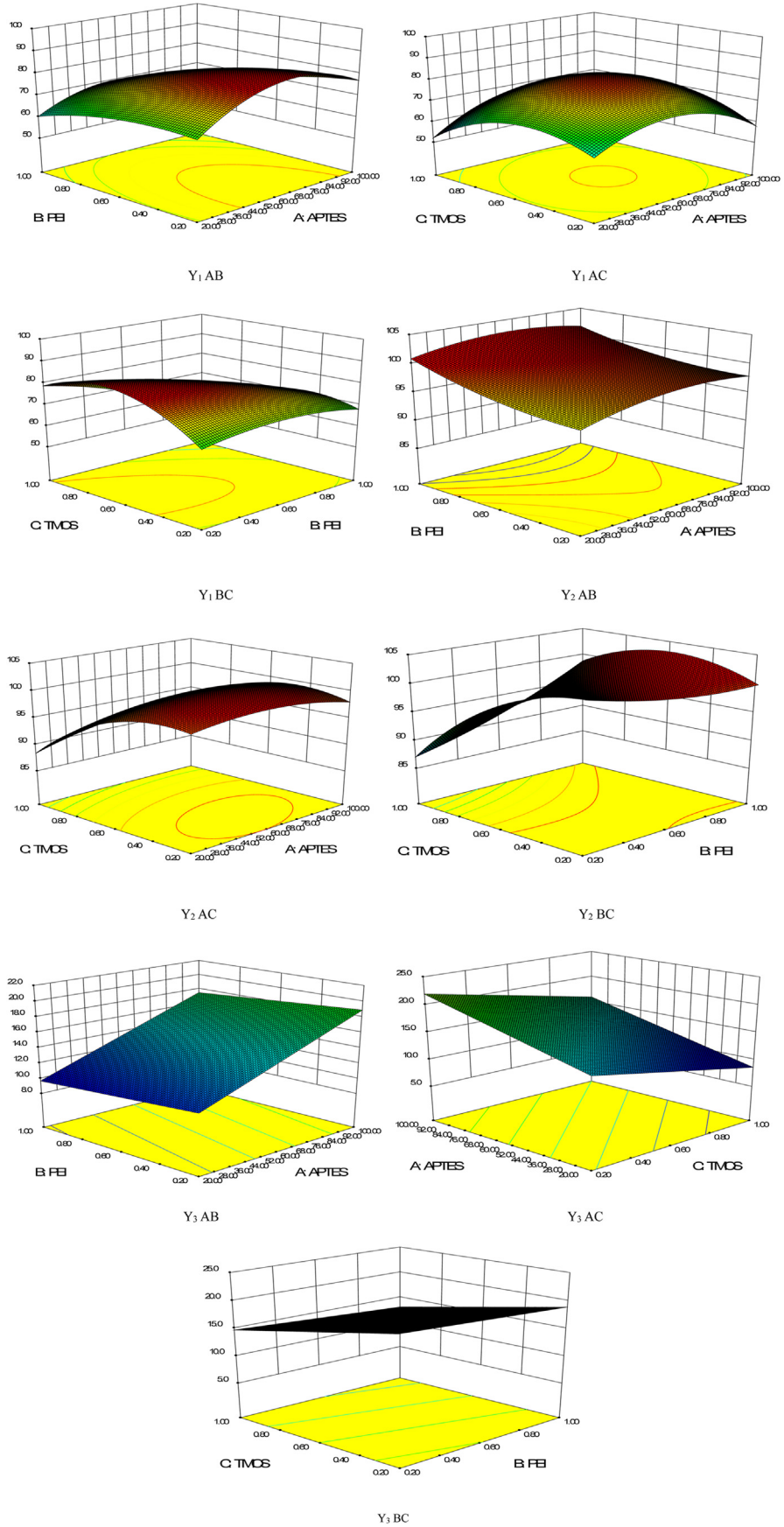

Fig. 7. Response surface plots showing effects of various independent variables on response Y_1, Y_2 and Y_3. X_1 is factor of APTES amount (μl), X_2 is factor of PEI amount (ml), X_3 is factor of TMOS amount (ml), Y_1 is response of cumulative drug release in 1 h (%), Y_2 is response of cumulative drug release in 24 h (%), Y_3 is response of drug loading capacity (%).

Table 6
The optimized LOFL-AMSX with the observed and predicted response values for different strengths. Y_1 is response of cumulative drug release in 1 h (%), Y_2 is response of cumulative drug release in 24 h (%), Y_3 is response of drug loading capacity (%).

No.		1	2	3
APTES (μl)		100	100	100
PEI (ml)		0.01	0.01	0.01
TMOS (ml)		0.01	0.02	0.05
Y_1	Predicted	–	–	40.3346
	Observed	–	–	39.3
Y_2	Predicted	–	–	103.397
	Observed	–	–	99.7
Y_3	Predicted	–	–	23.7
	Observed	–	–	23.3
Desirability		0.536	0.533	0.521

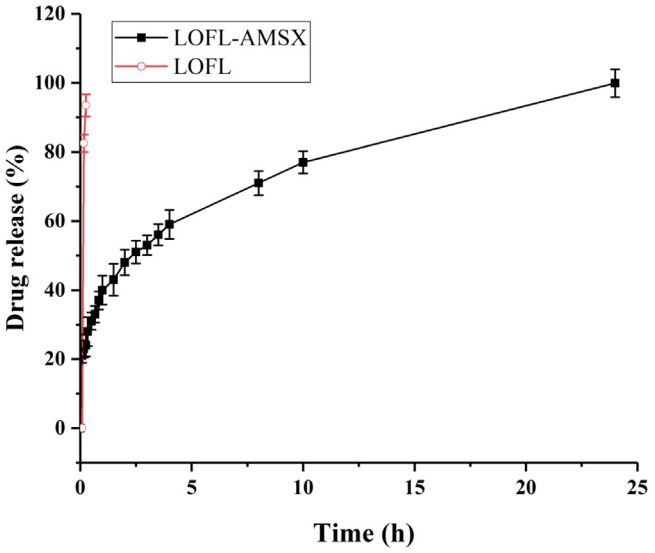

Fig. 8. Release profiles of LOFL and LOFL-AMSX.

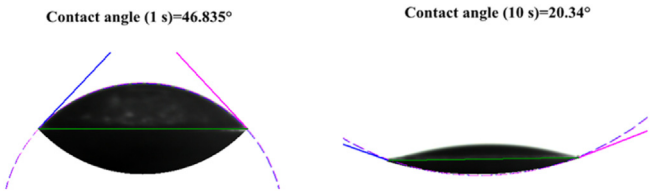

Fig. 9. Contact angle of LOFL-AMSX in 1 s and 10 s.

The resulted design of optimized sample 3 confirmed some conclusions made in the above discussion. Briefly, low dosage of PEI (0.01 ml) and TMOS (0.05 ml) were applied because polymer PEI had strong reaction ability to interact with silicon hydroxyl groups. TMOS could efficiently incorporate drug molecules with low dosage due to its strong hydrolysis and polycondensation properties [36,37]. High dosage of APTES (100 μl) contributed to high drug loading capacity since the high quantity of amino groups grafted onto the mesoporous silica adsorbed larger amount of carboxyl-containing drug molecules through hydrogen bonding. To confirm the validity of the calculated optimized factors and predicted responses, the drug release profiles of optimized LOFL-AMSX were carried out in triplicate (Fig. 8). Compared with LOFL release, LOFL-AMSX sustained LOFL release for 24 h because LOFL that loaded in the mesopores of AMSX was remained in one-piece xerogel. The xerogel functioned as drug reservoir and drug released gradually from mesopores into dissolution medium. Optimized LOFL-AMSX with relative low cumulative release in 1 h (39.3%) and high drug loading capacity (23.3%) was achieved. Further, the observed response values of LOFL-AMSX were close to predicted response values, confirming the good predictability and desirability of the three-level three-factorial Box–Behnken experimental design.

3.4.4. *Interfacial wetting behavior*

Fig. 9 showed the contact angle of optimized LOFL-AMSX at 1 s and 10 s, respectively. It turned out that the contact angle reduced from 46.835° to 20.34° during the short period time of 10 s, reflecting that the wettability of LOFL loaded AMSX increased with time. A drop of water can be wetted into AMSX powder in 11 s (Fig. 10), demonstrating the porosity of AMSX can load and store drug molecules. Thus, it was clear that the loaded drug in AMSX can be wetted with the entrance of aqueous medium and then released out from the carrier, which suggested the diffusion of drug loaded AMSX was mainly attributed to the porosity of AMSX. It also confirmed that the release mechanism of LOFL-AMSX was drug-controlled [38], which was a crucial point when studying AMSX as the excipient of solid dispersions. The mechanism can be described that dissolution into the diffusion layer of AMSX was comparatively slow and the drug released as solid particles. Consequently, the dissolution will not only be associated with the porosity and amino modification of AMSX but also be dominated by the properties (size, physical form, etc.) of drug itself. This may still lead to considerable improvements in dissolution compared to conventional dosage forms due tothe potential capacity of AMSX in regulating wettability and drug release behaviors.

4. Conclusion

The presented paper studied the facile synthesis of AMSX using co-condensation method and its potential value as drug carrier. Results of SEM, TEM, nitrogen adsorption/desorption and XPS measurements demonstrated that AMSX was accumulational spherical nanoparticles with mesoporous structure. FTIR result confirmed that hydrogen bonding force was formed between LOFL and AMSX. Several major conclusions were made from Box–Behnken experimental design to learn how AMSX regulated loading and in vitro release of LOFL: (1) APTES displayed positive impact on LOFL loading capacity because more amino groups grafted onto the mesoporous silica adsorbed larger amount of carboxyl-containing drug molecules through strong hydrogen bonding; (2) A small amount of PEI was sufficient to synthesize AMSX since the polymer PEI had strong reaction ability to interact with silicon hydroxyl groups; (3) TMOS could efficiently incorporate drug molecules with low dosage due to its strong hydrolysis and polycondensation properties. The optimized LOFL-AMSX sustained LOFL release for 24 h and could achieve relative low cumulative release in 1 h and high drug loading capacity. It is convincible that this research will be of significant help in designing optimized mesoporous silica xerogel as drug carrier and providing novel insight in the study of mesoporous silica and sustained release system.

Appendix A. Supplementary data

Supplementary data to this article can be found online at https://doi.org/10.1016/j.msec.2019.110266.

Fig. 10. Contact angle of AMSX from 0s to 11s.

References

[1] S. Dutta, A. Bhaumik, K.C.W. Wu, Energy Environ. Sci. 7 (2014) 3574–3592.
[2] F.-K. Shieh, S.-C. Wang, C.-I. Yen, C.-C. Wu, S. Dutta, L.-Y. Chou, J.V. Morabito, P. Hu, M.-H. Hsu, K.C.W. Wu, C.-K. Tsung, J. Am. Chem. Soc. 137 (2015) 4276–4279.
[3] F.-K. Shieh, C.-T. Hsiao, H.-M. Kao, Y.-C. Sue, K.-W. Lin, C.-C. Wu, X.-H. Chen, L. Wan, M.-H. Hsu, J.R. Hwu, C.-K. Tsung, K.C.W. Wu, RSC Adv. 3 (2013) 25686–25689.
[4] K.K. Qian, R.H. Bogner, J. Pharm. Sci. 101 (2012) 444–463.
[5] J. Li, L. Xu, B. Yang, H. Wang, Z. Bao, W. Pan, S. Li, Int. J. Pharm. 492 (2015) 191–198.
[6] J. Li, X. Du, N. Zheng, L. Xu, J. Xu, S. Li, Colloids Surfaces B Biointerfaces 141 (2016) 374–381.
[7] J. Andersson, J. Rosenholm, S. Areva, M. Lindén, Chem. Mater. 16 (2004) 4160–4167.
[8] T. Heikkilä, J. Salonen, J. Tuura, N. Kumar, T. Salmi, D.Y. Murzin, M. Hamdy, G. Mul, L. Laitinen, A. Kaukonen, Drug Deliv. 14 (2007) 337–347.
[9] L. Hu, H. Sun, Q. Zhao, N. Han, L. Bai, Y. Wang, T. Jiang, S. Wang, Mater. Sci. Eng. C 47 (2015) 313–324.
[10] V. Mamaeva, C. Sahlgren, M. Linden, Adv. Drug Deliv. Rev. 65 (2013) 689–702.
[11] J. Li, L. Xu, N. Zheng, H. Wang, F. Lu, S. Li, Mater. Sci. Eng. C 58 (2016) 1105–1111.
[12] P.N. Durfee, Y.S. Lin, D.R. Dunphy, A.J. Muniz, K.S. Butler, K.R. Humphrey, A.J. Lokke, J.O. Agola, S.S. Chou, I.M. Chen, W. Wharton, J.L. Townson, C.L. Willman, C.J. Brinker, ACS Nano 10 (2016) 8325–8345.
[13] R.H. Jin, J.J. Yuan, Macromol. Chem. Phys. 206 (2005) 2160–2170.
[14] J.J. Yuan, R.H. Jin, Adv. Mater. 17 (2005) 885–888.
[15] J. Li, H. Wang, H. Li, L. Xu, Y. Guo, F. Lu, W. Pan, S. Li, Int. J. Pharm. 498 (2016) 32–39.
[16] P.A. Patel, J. Eckart, M.C. Advincula, A.J. Goldberg, P.T. Mather, Polymer 50 (2009) 1214–1222.
[17] F. Tan, Q. Zhao, F. Teng, D. Sun, J. Gao, X. Quan, J. Chen, Mater. Lett. 129 (2014) 95–97.
[18] M. Sumper, N. Kröger, J. Mater. Chem. 14 (2004) 2059–2065.
[19] B. Tzankov, K. Yoncheva, M. Popova, A. Szegedi, G. Momekov, J. Mihály, N. Lambov, Microporous Mesoporous Mater. 171 (2013) 131–138.
[20] J. Li, L. Xu, H. Liu, Y. Wang, Q. Wang, H. Chen, W. Pan, S. Li, Int. J. Pharm. 467 (2014) 9–18.
[21] M. Xie, H. Shi, Z. Li, H. Shen, K. Ma, B. Li, S. Shen, Y. Jin, Colloids Surfaces B Biointerfaces 110 (2013) 138–147.
[22] I.I. Slowing, B.G. Trewyn, S. Giri, V.Y. Lin, Adv. Funct. Mater. 17 (2007) 1225–1236.
[23] S. Wang, Microporous Mesoporous Mater. 117 (2009) 1–9.
[24] J. Li, L. Xu, B. Yang, Z. Bao, W. Pan, S. Li, Mater. Sci. Eng. C 55 (2015) 367–372.
[25] A.A. Abdelbary, M.H.H. AbouGhaly, Int. J. Pharm. 485 (2015) 235–243.
[26] H.R. Naghibi Beidokhti, R. Ghaffarzadegan, S. Mirzakhanlouei, L. Ghazizadeh, F.A. Dorkoosh, AAPS PharmSciTech 18 (2017) 115–129.
[27] J.Z. Yanzhuo Zhang, Tongying Jiang, Siling Wang, Int. J. Pharm. 410 (2011) 118–124.
[28] J. Li, L. Xu, H. Wang, B. Yang, H. Liu, W. Pan, S. Li, Mater. Sci. Eng. C 59 (2016) 710–716.
[29] W. Zhu, L. Wan, C. Zhang, Y. Gao, X. Zheng, T. Jiang, S. Wang, Mater. Sci. Eng. C 34 (2014) 78–85.
[30] Y. Wang, N. Han, Q. Zhao, L. Bai, J. Li, T. Jiang, S. Wang, Eur. J. Pharm. Sci. 72 (2015) 12–20.
[31] J. Pang, L. Zhao, L. Zhang, Z. Li, Y. Luan, J. Colloid Interface Sci. 395 (2013) 31–39.
[32] Y. Hu, J. Wang, Z. Zhi, T. Jiang, S. Wang, J. Colloid Interface Sci. 363 (2011) 410–417.
[33] S.-W. Song, K. Hidajat, S. Kawi, Langmuir 21 (2005) 9568–9575.
[34] Y. Hu, Z. Zhi, T. Wang, T. Jiang, S. Wang, Eur. J. Pharm. Biopharm. 79 (2011) 544–551.
[35] M. Manzano, V. Aina, C.O. Areán, F. Balas, V. Cauda, M. Colilla, M.R. Delgado, M. Vallet-Regí, Chem. Eng. J. 137 (2008) 30–37.
[36] M. Ahola, P. Kortesuo, I. Kangasniemi, J. Kiesvaara, A. Yli-Urpo, Int. J. Pharm. 195 (2000) 219–227.
[37] J. Li, L. Xu, H. Wang, B. Yang, H. Liu, W. Pan, S. Li, Materials science & engineering, C, Materials for biological applications 59 (2016) 710–716.
[38] D.Q.M. Craig, Int. J. Pharm. 231 (2002) 131–144.